Learning & Perception 5 (2013) Suppl. 2, pp. 119–148
DOI: 10.1556/LP.5.2013.Suppl2.8

CLOSURE ENHANCEMENT IN A MODEL NETWORK WITH ORIENTATION TUNED LONG-RANGE CONNECTIVITY

BEÁTA REIZ[1,2,3], RÓBERT BUSA-FEKETE[4,5], SÁNDOR PONGOR[1,3,6] and ILONA KOVÁCS[7,8,*]

[1]International Centre for Genetic Engineering and Biotechnology, Padriciano 99 34129 Trieste, Italy
[2]Biological Research Centre, Hungarian Academy of Sciences, Temesvári krt. 62, H-6726 Szeged, Hungary
[3]Institute of Informatics, University of Szeged, Aradi vértanúk tere 1, H-6720 Szeged, Hungary
[4]HAS–SzTE Research Group on Artificial Intelligence, University of Szeged, Tisza Lajos krt. 103, H-6720 Szeged, Hungary
[5]Laboratoire de l'Accélérateur Linéaire, Université de Paris-Sud, CNRS, 91898 Orsay, France
[6]Faculty of Information Technology, Pázmány Péter Catholic University Práter u. 50, H-1083 Budapest, Hungary
[7]Department of Cognitive Science, Budapest University of Technology and Economics, Stoczek u. 2, H-1111 Budapest, Hungary
[8]HAS–BME Research Group in Cognitive Science, Budapest University of Technology and Economics, Stoczek u. 2, H-1111 Budapest, Hungary

The primary visual cortex (V1) of the mammalian brain is equipped with a specifically connected network of neurons that can potentially solve difficult image processing tasks. These neurons are selectively tuned for locations in visual space and also for line orientation. The coupling of location and orientation tuning results in the neural representation of the visual world in terms of local features. These local features, e.g., oriented line segments, will have to be linked together in order to parse the visual world into regions corresponding to object and ground. Although standard models of V1 do not address the issue of interacting neuronal populations, we suggest that the long-range connectivity pattern of V1 provides an architecture where spreading neural activity may lead to pertinent figure-ground segmentation. The model relies on the fact that in addition to the processing units, their connections

* Corresponding author: Ilona Kovács, Department of Cognitive Science, Budapest University of Technology and Economics, Stoczek u. 2, Budapest, H-1111 Hungary

are also selectively tuned for space and orientation. From the computational point of view, the model uses a minimalist approach that applies the fundamental concepts of Gestalt psychology – proximity, similarity and continuity – to the spreading of neuronal activation signals. This model is successful in predicting psychophysical performance of human observers, and provides an account of the computational power of V1.

Keywords: primary visual cortex, minimalistic model, contour integration

INTRODUCTION

Among the many unsolved issues of visual information processing, the issue of segmentation is among the thorniest ones *(Figure 1)*. Ambiguities arise because the local feature detectors, working in terms of local rules of grouping, are not able to take into consideration the global properties of an image. A certain local, neighbor-to-neighbor connection might be reasonable in local terms, however, it might not work in terms the global composition of the image. These ambiguities would lead to bi- and multi-stable image interpretations, however, the human visual system seems to cope with the most ambiguous situations. Although computer

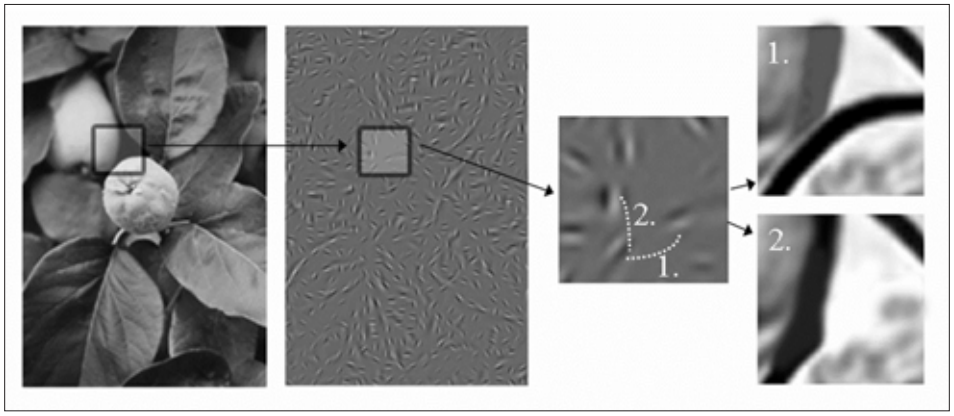

Figure 1. The cortical puzzle. According to the "standard" view of low-level visual processing, simple cells in the primary visual cortex compute a linearly weighted sum of the input over space and time with a Gabor-like function, followed by response normalization. The second panel shows the most activated hypothetical filters for each location within the image. The local filter bank, however, only provides locally interpretable results, and the pieces will need to be linked together. There is an inherent ambiguity in grouping local elements, as the insets show. Which one is a good connection – 1 or 2? The central object will be well segmented by choosing 1, however, 2 would be a very bad choice, connecting the boundaries of two independent objects. Beyond the "standard" view, it is assumed that neural interactions within the primary visual cortex connect the local filters in an orientation- and position-selective (e.g., similar-to-similar orientations, and along smooth curves) facilitatory manner, providing a basic tool for solving the puzzle illustrated here.

vision systems still cannot match the capabilities of the human visual system in parsing a visual image into regions corresponding to object and ground, building upon the known long-range connectivity pattern of the visual cortex, we demonstrate that spreading activity in a simplified neural network may lead to pertinent bottom-up segmentation and noise elimination when both the processing units and their connections are selectively tuned for space and orientation. We model spreading activity as a finite Markov chain with the transition matrix based on the weighted link structure. The uniqueness of this approach is that while the model only specifies local information (such as edge orientation; proximity and co-linearity of neighboring edge segments; or local smoothness of curves) global properties, such as contour closure and segmentation emerge.

According to the "standard" view of visual processing, retinal input is conveyed through several parallel pathways to the brain in a compressed edition, emphasizing edge information at a number of spatial scales. A fundamental step is carried out by cortical area 17 (V1, or primary visual cortex) that is assumed to extract a set of features. It has been known for over 40 years that the shape and layout of neuronal receptive fields in V1 furnish the cells with selectivity for oriented line segments, and receptive field size determines the spatial scale of orientation information (Hubel & Wiesel, 1959). The primary visual cortex thus provides a neural description of oriented edge primitives and their locations at a number of spatial scales. This can be viewed as an enormous puzzle containing countless pieces to be put together into figure and ground *(Figure 1)*. Beyond the scope of the "standard" view, a possible candidate for assembling local information already within the primary visual cortex is the plexus of long-range horizontal axonal connections (Gilbert, 1992; Gilbert & Wiesel, 1989; Rockland & Lund, 1983; Rockland, Lund, & Humphrey, 1982) that connect neurons responding to different spatial positions, however, with similar tuning properties. The intrinsic (within cortical area V1) intralaminar (horizontal) connections start off primarily from layer 2/3 pyramidal cells with a 2–5 mm extension parallel to the cortical surface, and terminate in a patchy manner with excitatory synapses (Gilbert & Wiesel, 1989; Rockland et al., 1982). A high level of selectivity, in terms of for example, local orientations, is behind the generally observed patchy nature of horizontal connections. The clustered projections have been shown to connect neuronal populations with similar orientation preference (Angelucci et al., 2002; Bosking, Crowley, & Fitzpatrick, 2002; Bosking, Zhang, Schofield, & Fitzpatrick, 1997; Gilbert & Wiesel, 1989; Kisvarday & Eysel, 1992; Stettler, Das, Bennett, & Gilbert, 2002), with an estimated bandwidth of about 60 degrees (Stettler et al., 2002). The neural representation of visual space in V1 is known to be retinotopic. However, the relationship between the retinotopic map, and the orientation selectivity of long-range intrinsic connections has only been addressed by a single study, that of Bosking et al. (Bosking et al., 1997). Here it was demonstrated that there is an orientation-specific visuotopic anisotropy, indicating that the connections prefer neurons that are both co-oriented and co-axial, but also allow for connections lacking the latter.

In order to test the computational power of neurons with conjoint orientation preference in the primary visual cortex, a behavioral paradigm has been developed, involving a contour-in-noise stimulus (Kovacs & Julesz, 1993). The contour integration (CI) stimulus is composed of randomly positioned local orientation signals (Gabor patches) that are optimal stimuli for V1 orientation-tuned neurons, and a set of these Gabor signals are arranged along a contin-

uous contour path with various shape properties (see Figure 3; a similar paradigm, although not allowing for variations in shape, was developed in parallel by Field and his associates (Field, Hayes, & Hess, 1993). In addition to the constraints in the design that particularly make it suitable for studies on low-level cortical long-range connectivity, neural correlates indicate the relevance of low-level visual areas in the detection of the contour-in-noise stimulus.. Such correlates involve the correspondence between neuronal and behavioral responses in monkeys (W. Li, Piech, & Gilbert, 2008), direct architectural data in monkeys (Stettler et al., 2002), optical imaging of contextual interactions in monkeys (Kinoshita, Gilbert, & Das, 2009), human neuropsychology (Giersch, Humphreys, Boucart, & Kovacs, 2000) and human fMRI studies (Altmann, Bulthoff, & Kourtzi, 2003; Kourtzi, Tolias, Altmann, Augath, & Logothetis, 2003). Based on these studies, the possible candidate for assembling local orientation information in CI is the plexus of long-range horizontal connections in V1. The presence of global, shape-dependent contextual processes in CI have been demonstrated (Kovacs, 1996; Kovacs & Julesz, 1993, 1994; W. Li & Gilbert, 2002; Mathes & Fahle, 2007), indicating that long-range connectivity might contribute to object related processing in V1 well beyond local feature analysis.

Computational models may help to clarify the potential processing capacity of the selectively tuned intrinsic long-range connectivity pattern of V1 with respect to image segmentation. There have been a variety of attempts to model this network, either relying on realistic neuronal properties (Z. Li, 1998, 2005; Yen & Finkel, 1998), or, at a more abstract level, concentrating on contour integration (August & Zucker, 2003; Mumford, 1993; Williams & Jacobs, 1997). In simplified modeling accounts, a generally accepted view exists – based on the suggestions of David J. Field (Field et al., 1993) and William H. Bosking (Bosking et al., 1997) and their associates – that the "association field" of local orientation detectors is anisotropic for space, and long-range facilitatory connections are always co-axial. However, although the actual anatomical data indicate co-axial connectivity, other types of connections are not excluded, given that they are orientation selective – see for example (Bosking et al., 1997; Stettler et al., 2002). We argue that the orderly architecture of V1 allows for a coupled representation of space and orientation where co-axial and non-co-axial connections may have different weights.

Our purpose here is to put the known properties of V1 long-range connectivity to a test, and shed light on their computational capacity. The abstract model described here aims at reproducing only the main features of this network: local orientation measurements, orientation- and distance selective connections, and spreading neural activity. We use a Markovian model which has been suggested earlier to model interactions of this sort, where the state of each unit depends on the state of neighboring units and not on the state of all units (August & Zucker, 2003; Mumford, 1993; Williams & Jacobs, 1997). Our assumption is that the image emerging in V1 corresponds to the convergence point of a Markovian system. Test images are the same contour-in-noise images that were used in the psychophysical experiments, including both closed and open contours (Kovacs & Julesz, 1993). The chain of interactions in the model network converges very fast to a segmented image, and the efficiency of segmentation with closed versus open contours resembles that of the human performance (Kovacs & Julesz, 1993).

RESULTS

Test contours

In order to be able to directly address the issue of V1 connectivity, we employed the contour-in-noise stimuli used in a number of behavioral, physiological, imaging and modeling studies (Altmann et al., 2003; Giersch et al., 2000; Kourtzi et al., 2003; Kovacs, 1996; Kovacs & Julesz, 1993, 1994; W. Li & Gilbert, 2002; W. Li et al., 2008; Z. Li, 1998, 2005; Mathes & Fahle, 2007; Yen & Finkel, 1998). The test set of contours was composed of the so-called Gabor patches (GPs) that model the receptive fields of simple cells. Contiguous contours were generated, consisting of 13–14 GPs, and placed at a distance of 7–8 times the wavelength-units (lambda) from each other. To each contour, a varying number of randomly placed GPs were added as background noise, resulting in a set of contours embedded in an increasing amount of noise (see *Figure 3* below and Supporting Information 1). The full set of the open versus closed contours used in evaluating our model can be seen in *Figures S1–15*.

Contour integration algorithm

The main idea underlying the model is that the image is mapped onto the visual cortex in a retinotopic manner, and local orientation information is assembled by *spreading activity* through selectively tuned connections. Activation spread is controlled by the *proximity* of activated units, the *similarity* of orientation tuning and the *continuity* of longer chains of activation. The simplest way to put these ideas into a mathematical model is to imagine the activated units as nodes of a network, and the spreading neuronal activity as links between the nodes. A threshold-based mathematical form is used to define the network as it is illustrated in *Figure 2*. Links form if two nodes are closer than a length threshold *L* (proximity

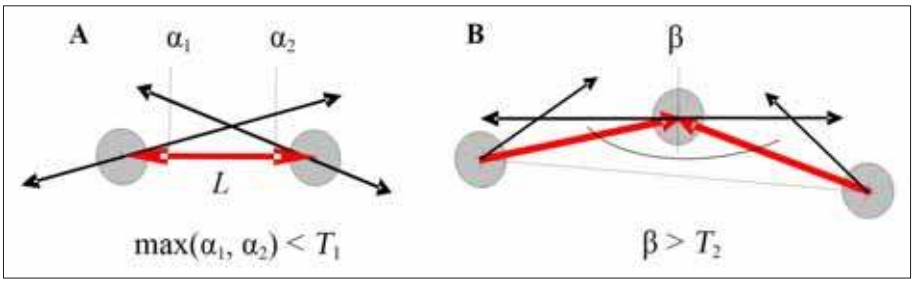

Figure 2. The principle of geometric filtering used by the model. (A) Preprocessing. At this stage, two Gabor patches are considered linked (red line) if their distance *L* is below a proximity threshold (proximity filtering) and if angle α_1 and α_2 are below an orientation similarity threshold T_1 (similarity filtering). The angles α_1 and α_2 are defined in such a way that our similarity filter checks for the similarity of the orientations and the supporting line of the examined GPs. (B) Continuity Filtering. At this stage, three Gabor patches are considered linked (two bold lines), if their angle is above a continuity threshold T_2. During the calculations, (A) is done once at the beginning while (B) is repeated before every propagation step.

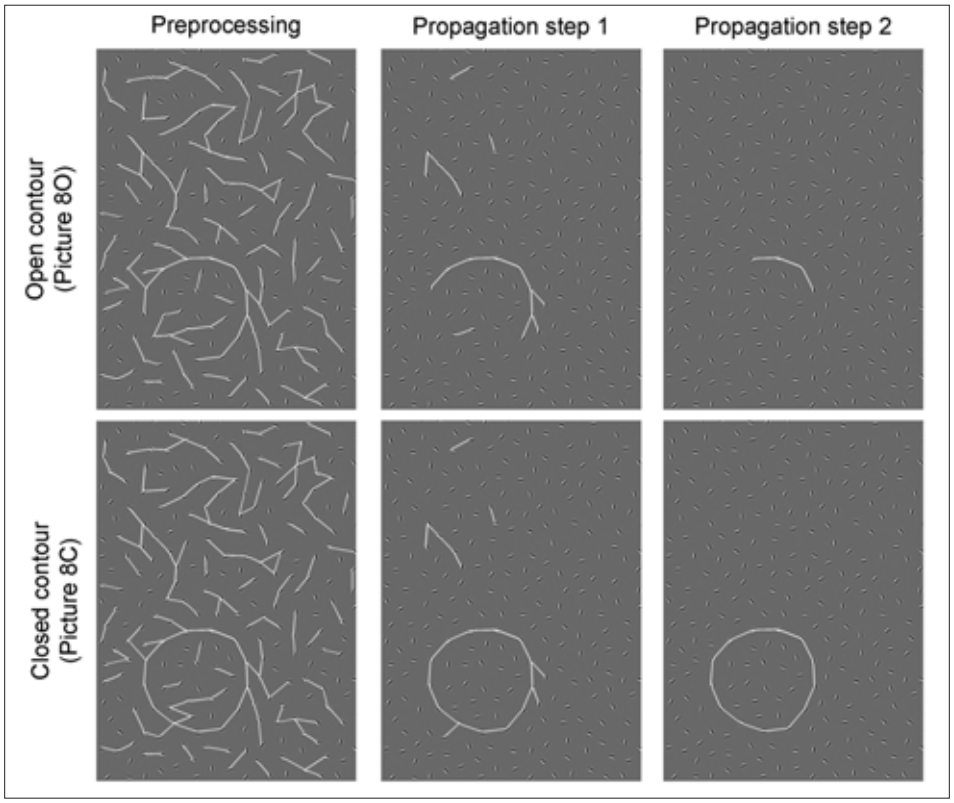

Figure 3. The step-by-step results of the algorithm with images containing open (top panels) versus closed (bottom panels) contours. Images 8O and 8C (see *Figure S8*) are of intermediate difficulty for human observers.

constraint), the angle of the local orientations is below a threshold T_1 (similarity constraint; see *Figure 2A*), and if the angle of links pointing to the same activated node is close enough to the straight angle (continuity constraint, see *Figure 2B*). We assume that neuronal activity spreads among the activated nodes in an essentially random fashion that we model as a finite Markov chain with a transition matrix based on the weighted link structure.

The algorithm is implemented in two phases:

1. Preprocessing (Proximity and Similarity Filtering). The input data (see *Figures S1–15*) are transformed into an initial interaction network in which the nodes are the orientation-tuned units, and the edges represent facilitatory neuronal activation. Edges are formed when the distance between two nodes is shorter than a distance threshold L and their similarity value *(Figure 2A)* is below a threshold T_1. This yields a relatively sparse network of initial connections *(Figure 3)*.

2. Continuity Propagation. In this phase, we first weight the edges of the network, and then iteratively propagate the weights using a random walk algorithm. The weights w_{ij} are computed from the number of continuous (collinear) edge-pairs cp_{ij} a particular edge partici-

pates in. Two edges are considered continuous if their angle is close enough to the straight angle – above a threshold T_2 (*Figure 2B*). As the number of edges changes during the iterations, we recalculate cp_{ij} in every step as shown in section Materials and Methods. As a result of the propagation, some edges of the network will amplify while others fade away. Typically, the edges representing continuous patterns remain, while randomly emerging noise disappears, so the result is a graph that contains only the edges belonging to the perceived pattern *(Figure 3)*. We note that the activation is strictly local; it depends on signals received by the individual nodes. No complex relationships (such as link triplets) are necessary. We also note that the weights of the links correspond to signal strength, and not to neural connectivities. The changes in activation thus reflect the dynamics of the system which is approximately described as a Markov process.

The performance of the model is characterized by a so-called *F*-measure used in statistics that is calculated from the number of correctly identified edges in the pattern (*TP*), the number of erroneously identified edges in the background (*FP*), and the number of edges not identified along the contour (*FN*). The *F*-measure is then calculated as $F = 2TP/(2TP + FN + FP)$ which results in a value between 0 and 1.0. When $F = 1.0$ a pattern is identified without errors (e.g., the pattern shown in *Figure 3*). We found that the threshold values of the parameters: $L = 7–12\ \lambda$, $T_1 = 30–50$ degrees, and $T_2 = 100–160$ degrees gave correct results after a few steps of iteration, i.e., the circular patterns appeared without any errors *(Figure S7C)*. The tightness of the threshold only affects the required number of propagation steps necessary to reach convergence: the tighter the thresholds, the fewer propagation steps are required for the pattern to appear without any errors. We used the tightest threshold settings

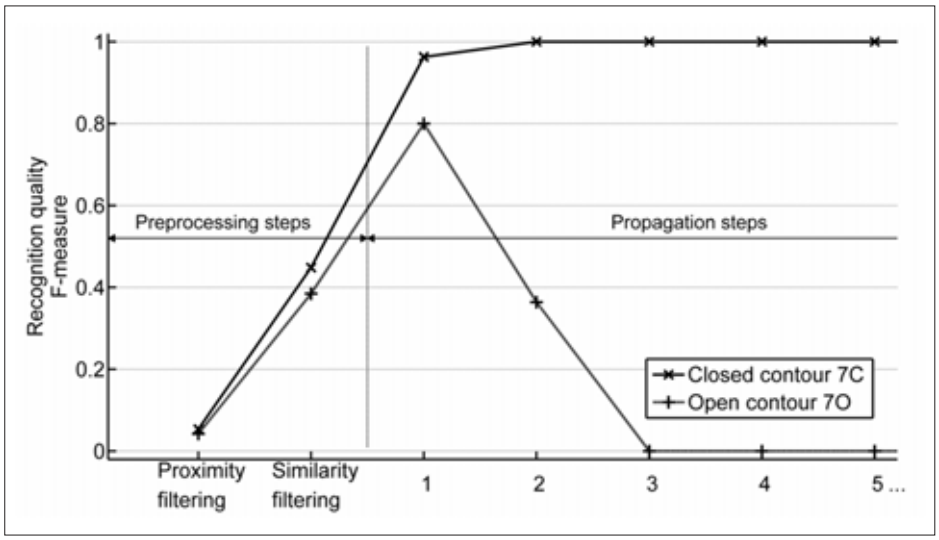

Figure 4. Recognition quality expressed in *F*-measure (see text) of open and closed contours in sequential phases of the algorithm. The contour numbers 7C and 7O refer to *Figure S7*. The algorithm carries out the steps in the order indicated on the *x* axis.

for all images, and averaged the performance after rotating the images by 5° until a full 360° rotation was completed. The tightest thresholds for each image were selected separately in such a manner that we assured all GPs from the pattern met all filtering criteria.

Open versus Closed contours

Figure 4 illustrates the changes in recognition quality (*F*-measure) of a closed and an open contour throughout the preprocessing and propagation steps of the algorithm. The closed contour is amplified, while the open contour fades away, which is a result of propagation, i.e., spreading activation through the network. Notice that only a few (1–2) propagation steps are needed for perfect recognition of the closed contour. The fact that the recognition quality (*F*-measure) of the open contour vanishes after a few propagation steps does not mean that open contours are not perceived. It simply means that the activation dynamics are very different for open and closed contours. No assumptions are made on how the information is further processed.

As described in the Materials and Methods section, we systematically varied the amount of background noise for both open and closed contours. *Figure 5* summarizes the effects of

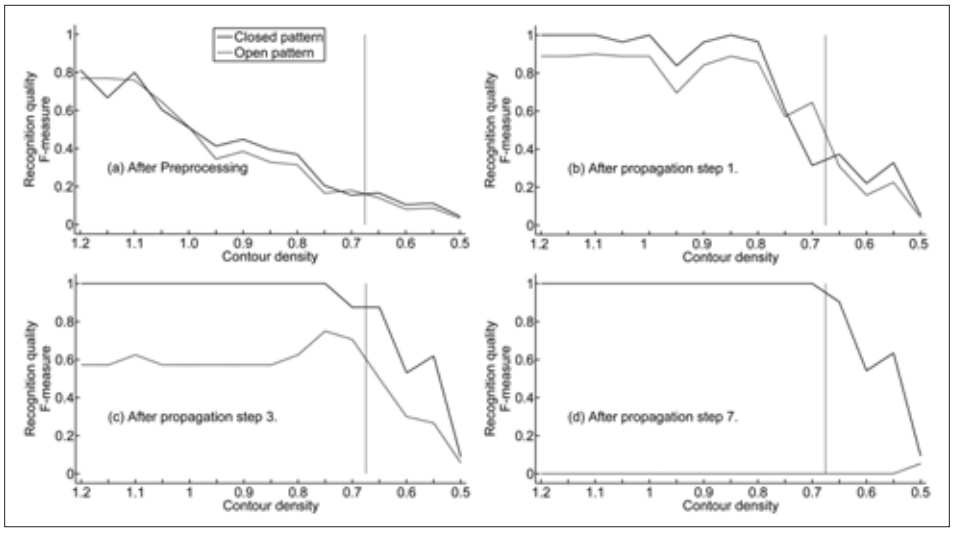

Figure 5. Comparison of recognition quality on open and closed contour images of increasingly dense noise backgrounds. The numbers on the *x* axes are the contour densities of the open and closed contour images, and indicate that the background noise increases from higher to lower contour densities (see *Figures S1–15*). The vertical line drawn at about 0.725 corresponds to the average human recognition performance seen in earlier studies (Kovacs & Julesz, 1993). Recognition quality was measured after (a) the preprocessing step; (b) the 1st propagation step; (c) the 3rd propagation step; (d) the 7th propagation step. Note that the difference between the closed contours (continuous line) and open contours (dashed line) increases upon propagation.

noise on recognition quality after preprocessing and propagation. Lower levels of noise clearly lead to better recognition of both open and closed contours at the preprocessing level. However, propagation affects them differently. Closed contours are enhanced, and those with higher levels of noise become correctly recognized with more propagation steps. Open contours fade away as propagation goes on. The difference between closed patterns (continuous line) and open patterns (dashed line) increases with propagation. Human threshold performance for closed contours (Kovacs & Julesz, 1993) is indicated by the vertical line.

DISCUSSION

We presented a highly simplified computational model that contains only three basic features of the long-range connectivity network of the primary visual cortex (V1): local orientation measurements, orientation and distance selective connections, and spreading neural activity. Our model is built on two mathematical conditions: threshold based selection of connections and propagation of neural activity. We found that this simplified network model is capable of detecting contours in a noisy background, with sensitivity to background noise and a preference for closed contours that resemble human performance (Kovacs & Julesz, 1993).

Standard models of V1 do not address the issue of interacting neuron populations (Olshausen & Field, 2005), suggesting that they are not relevant in predicting psychophysical performance in contour integration studies, and therefore cannot provide an account of the full computational power of V1. The "association field" idea of David J. Field and his associates (Field et al., 1993) includes the first preprocessing phase of our model, where local interactions are biased towards co-oriented and co-axial filters. However, the propagation phase implemented by our algorithm has not been suggested earlier. In terms of the actual anatomical connectivity of V1, a bias towards co-oriented and co-axial long-range connections of layer 2/3 pyramidal neurons have been convincingly demonstrated (Bosking et al., 1997), although the presence of non-coaxial connections is also obvious (see, e.g., Figure 4 in (Bosking et al., 1997)). We suggest that continuity propagation might be mediated with such an architecture, where co-oriented connections are weighted differently for co-axial and non-coaxial retinotopic arrangements. We mention that from the computational point of view, our model uses a minimalist approach that applies the fundamental concepts of Gestalt psychology – proximity, similarity and continuity – to the spreading of neuronal activation signals.

Our model suggests that the properties of long-range facilitatory connections should be further tested in V1, with a particular emphasis on the exact tuning of these interactions for both orientation and space. Since the model produced global effects, such as a preference for contour closure, it would be interesting to see whether shape-related effects – as described in (Kovacs, 1996; Kovacs, Feher, & Julesz, 1998; Kovacs & Julesz, 1994) – can be a consequence of such a connectivity pattern as well.

Long-range lateral intralaminar connections between pyramidal cells seem to be a ubiquitous feature of the superficial cortical layers across species. Such connections have been

observed in cat (Gilbert & Wiesel, 1989; Kisvarday & Eysel, 1992); tree shrew (Rockland et al., 1982); and monkey (Rockland & Lund, 1983), for example. It has recently been suggested that these long axonal projections shape the neocortex into "canonical circuits" serving spatiotemporal integration within the functional maps (Douglas & Martin, 2004, 2007; Tsodyks, Kenet, Grinvald, & Arieli, 1999). It remains to be seen what the computational power of finely tuned interactions is across different species, and different modalities.

In summary, we found that a model, implementing only a few important features of the processing layer in the primary visual cortex, such as local orientation measurements, orientation and distance selective connections and spreading neural activity, adequately predicts low-level image-segmentation characteristics of human vision.

MATERIALS AND METHODS

Test images

The test images listed in *Table 1* were generated by the method first described in (Kovacs & Julesz, 1993), and developed further in (Kovacs, Polat, Pennefather, Chandna, & Norcia, 2000).

Table 1. Codes and characteristics of the test images used in this study. The images and their main statistical parameters are in *Figures S1–15*.

Closed contour	Open contour	GP–GP distance D [λ units]		Relative density
		Background	Contour	($D_{background}/D_{contour}$)
1 C	1 O	8.4	7	1.20
2 C	2 O	8.1	7	1.16
3 C	3 O	7.7	7	1.10
4 C	4 O	7.4	7	1.06
5 C	5 O	7.0	7.1	0.99
6 C	6 O	6.7	7	0.96
7 C	7 O	6.3	7	0.90
8 C	8 O	5.9	7	0.84
9 C	9 O	5.6	7.1	0.79
10 C	10 O	5.2	7	0.74
11 C	11 O	4.9	7.1	0.69
12 C	12 O	4.5	7	0.64
13 C	13 O	4.2	7	0.60
14 C	14 O	3.8	7.2	0.53
15 C	15 O	3.5	7	0.50

Model

The input of the algorithm is an image composed of a set of Gabor patches, each patch being characterized by $r_i = (r_{ix}, r_{iy})$ coordinates in the plane and two coordinates, $d_i = (d_{ix}, d_{iy})$ of an orientation unit vector. The algorithm takes the Gabor patch data as input, and then calculates an interaction network in two phases:

1) Preprocessing (proximity and similarity filtering). We consider two Gabor patches linked by an edge within the network if the distance and orientation similarity (coaxiality) constraints defined in *Figure 2A* are met. This calculation yields a network ($G = (V, E)$ graph) whose adjacency matrix M contains values of 1 if two Gabor patches are linked and zero otherwise. We define the graph $G = (V, E)$, where V is the set of Gabor patches on the image, and the set of edges is E. An edge is considered between two Gabor patches v_i and v_j if and only if the two criteria below are met:

$$\left\| r_i - r_j \right\| < L\,, \qquad \text{(Proximity filter)}$$

$$\max\left(\angle\left(r_i r_j, d_i \right), \angle\left(r_i r_j, d_j \right) \right) < T_1\,, \qquad \text{(Similarity filter)}$$

where $r_i r_j$ denotes the line formed by the positions of the two (ith and jth) Gabor patches.

We will use the adjacency matrix M of the above constructed graph G in the next phase of the algorithm.

2) Continuity Propagation. This part of the algorithm consists of two phases: 2.1) Continuity weight computation – Algorithm 1: steps 1–2, and 2.2) Propagation – Algorithm 1: steps 3–5.

2.1. We first weight the edges of the starting interaction network. The weights w_{ij} are computed from cp_{ij}, which is the number of continuous (collinear) edge pairs a particular edge participates in, according to the following formula:

$$cp_{ij} = \mathrm{card}\left(CP_{ij} \right),$$

where

$$CP_{ij} = \left\{ v_k \,\middle|\, \max\left(\angle\left(r_i r_j, r_j r_k \right) \right) > T_2, m_{ij} \neq 0, m_{jk} \neq 0 \right\}.$$

A particular edge can participate in more than one continuous edge-pairs, so the value of cp_{ij} equals the number of adjacent edges for which the continuity constraint *(Figure 2B)* is met ($0 \leq cp_{ij}$ number of adjacent edges). If no adjacent edges fulfil the constraint, the edge gets a weight w_{ij} of zero and is thus deleted; otherwise the weight gets the value of 1 if it is involved in a single continuous edge pair, and the value of 2 if it has at least two collinear edge pairs.

2.2. The weights w_{ij} are propagated on the network using an absorbing random walk model. After one propagation step, edges not fulfilling the absorption criteria are deleted. In each propagation step the occupancy of the nodes are computed (see step 4 in *Algo-*

rithm 1) and nodes with an occupancy value lower than 50% of the average occupancy are deleted.

We start with initializing a TM^0 matrix with the identity matrix, and define the occupancy values P^0 for all vertices equally (e.g. P^0 = 1/number of vertices). The above two steps are than repeated until convergence (see *Algorithm 1*). During the propagation phase, at each step, edges are deleted, and the calculation is terminated when the number of edges remains constant for two consecutive steps. In practice, this state is reached after at most 4–5 steps. Typical results are shown in *Figure 3* and further analysis of the algorithm is shown in Supporting Materials 2.

Algorithm 1. Continuity propagation algorithm

Initialize TM^0 with the identity matrix, and occupancy values P^0 = 1/number of vertices for each vertex.

repeat

1. compute cp_{ij} or all vertices v_i and v_j s.t. $m_{ij} \neq 0$.
2. define the weights m_{ij} of edges, than row-normalize the resulted weight matrix
$$w_{ij} = \begin{cases} 0, & \text{if} \quad cp_{ij} = 0 \\ 1, & \text{if} \quad cp_{ij} = 1 \\ 2, & \text{if} \quad cp_{ij} > 1 \end{cases}$$
3. propagation: $TM^{t+1} = TM^t \cdot w$
4. for every node v_i compute the occupancy as:
$$P_i^{t+1} = P_i^t \cdot \sum_{j \in \{v_j | m_{ij} \neq 0\}} TM_{ij}^{t+1}$$
5. for all v_i s.t. $P_i <$ threshold set $m_{ij} = 0$ for all v_j

until convergence

An iteration step can be subdivided into two conceptual phases: i) computation of the weighted link structure (steps 1., 2.), ii) Spreading of weights along the network (step 3.) and occupancy-based link deletion (steps 4., 5.)

ACKNOWLEDGEMENTS

BR is PhD student at the Informatics PhD Program of the University of Szeged, Hungary and at the ICGEB sandwich PhD program in Molecular Biology, Trieste, Italy. The work at BRC

Szeged was partly supported by a grant no TÁMOP-4.2.2-08/1/2008-008 from the Hungarian National Office for Research and Technology (NKTH) and by the National Science Foundation, Hungary (OTKA K. 84335). The work at Pázmány University was partially supported by NKTH grants TET_10-1-2011-0058, TÁMOP-4.2.1.B_11/2/KMR-2011-0002 and TÁMOP-4.2.2/B-10/1-2010-0014. IK was supported by the National Science Foundation, Hungary (OTKA NF60806) and the Social Renewal Program, Hungary (TÁMOP-4.2.2/08/1/KMR).

REFERENCES

Altmann, C. F., Bulthoff, H. H., Kourtzi, Z. (2003): Perceptual organization of local elements into global shapes in the human visual cortex. *Curr Biol, 13*(4), 342–349.

Angelucci, A., Levitt, J. B., Walton, E. J., Hupe, J. M., Bullier, J., Lund, J. S. (2002): Circuits for local and global signal integration in primary visual cortex. *J Neurosci, 22*(19), 8633–8646.

August, J., Zucker, S. W. (2003): Sketches with curvature: The curve indicator random field and Markov processes. *IEEE Trans. Pattern Anal. Mach. Intell., 25*(4), 387–400.

Bosking, W. H., Crowley, J. C., Fitzpatrick, D. (2002): Spatial coding of position and orientation in primary visual cortex. *Nat Neurosci, 5*(9), 874–882.

Bosking, W. H., Zhang, Y., Schofield, B., Fitzpatrick, D. (1997): Orientation selectivity and the arrangement of horizontal connections in tree shrew striate cortex. *J Neurosci, 17*(6), 2112–2127.

Douglas, R. J., Martin, K. A. (2004): Neuronal circuits of the neocortex. *Annu Rev Neurosci, 27*, 419–451.

Douglas, R. J., Martin, K. A. (2007): Mapping the matrix: the ways of neocortex. *Neuron, 56*(2), 226–238.

Field, D. J., Hayes, A., Hess, R. F. (1993): Contour integration by the human visual system: evidence for a local "association field". *Vision Res, 33*(2), 173–193.

Giersch, A., Humphreys, G. W., Boucart, M., Kovacs, I. (2000): The computation of occluded contours in visual agnosia: Evidence for early computation prior to shape binding and figure-ground coding. *Cogn Neuropsychol, 17*(8), 731–759.

Gilbert, C. D. (1992): Horizontal integration and cortical dynamics. *Neuron, 9*(1), 1–13.

Gilbert, C. D., Wiesel, T. N. (1989): Columnar specificity of intrinsic horizontal and corticocortical connections in cat visual cortex. *J Neurosci, 9*(7), 2432–2442.

Hubel, D. H., Wiesel, T. N. (1959): Receptive fields of single neurones in the cat's striate cortex. *J Physiol, 148*, 574–591.

Kinoshita, M., Gilbert, C. D., Das, A. (2009): Optical imaging of contextual interactions in V1 of the behaving monkey. *J Neurophysiol, 102*(3), 1930–1944.

Kisvarday, Z. F., Eysel, U. T. (1992): Cellular organization of reciprocal patchy networks in layer III of cat visual cortex (area 17). *Neuroscience, 46*(2), 275–286.

Kourtzi, Z., Tolias, A. S., Altmann, C. F., Augath, M., Logothetis, N. K. (2003): Integration of local features into global shapes: monkey and human FMRI studies. *Neuron, 37*(2), 333–346.

Kovacs, I. (1996): Gestalten of today: early processing of visual contours and surfaces. *Behav Brain Res, 82*(1), 1–11.

Kovacs, I., Feher, A., Julesz, B. (1998): Medial-point description of shape: a representation for action coding and its psychophysical correlates. *Vision Res, 38*(15–16), 2323–2333.

Kovacs, I., Julesz, B. (1993): A closed curve is much more than an incomplete one: effect of closure in figure-ground segmentation. *Proc Natl Acad Sci U S A, 90*(16), 7495–7497.

Kovacs, I., Julesz, B. (1994): Perceptual sensitivity maps within globally defined visual shapes. *Nature, 370*(6491), 644–646.

Kovacs, I., Polat, U., Pennefather, P. M., Chandna, A., Norcia, A. M. (2000): A new test of contour integration deficits in patients with a history of disrupted binocular experience during visual development. *Vision Res, 40*(13), 1775–1783.

Li, W., Gilbert, C. D. (2002): Global contour saliency and local colinear interactions. *J Neurophysiol, 88*(5), 2846–2856.

Li, W., Piech, V., Gilbert, C. D. (2008): Learning to link visual contours. *Neuron, 57*(3), 442–451.

Li, Z. (1998): A neural model of contour integration in the primary visual cortex. *Neural Comput, 10*(4), 903–940.

Li, Z. (2005): The Primary Visual Cortex Creates a Bottom-up Saliency Map. In I. Laurent, R. Geraint K. T. John (Eds.), *Neurobiology of Attention* (pp. 570–575): Academic Press, Burlington.

Mathes, B., Fahle, M. (2007): Closure facilitates contour integration. *Vision Res, 47*(6), 818–827.

Mumford, D. (1993): Elastica and Computer Vision. In C. Bajaj (Ed.), *Algebraic Geometry and its Applications* (pp. 507–518): Springer-Verlag.

Olshausen, B. A., Field, D. J. (2005): How close are we to understanding v1? *Neural Comput, 17*(8), 1665–1699.

Rockland, K. S., Lund, J. S. (1983): Intrinsic laminar lattice connections in primate visual cortex. *J Comp Neurol, 216*(3), 303–318.

Rockland, K. S., Lund, J. S., Humphrey, A. L. (1982): Anatomical binding of intrinsic connections in striate cortex of tree shrews (Tupaia glis): *J Comp Neurol, 209*(1), 41–58.

Stettler, D. D., Das, A., Bennett, J., Gilbert, C. D. (2002): Lateral connectivity and contextual interactions in macaque primary visual cortex. *Neuron, 36*(4), 739–750.

Tsodyks, M., Kenet, T., Grinvald, A., Arieli, A. (1999): Linking spontaneous activity of single cortical neurons and the underlying functional architecture. *Science, 286*(5446), 1943–1946.

Williams, L. R., Jacobs, D. W. (1997): Stochastic completion fields; a neural model of illusory contour shape and salience. *Neural Comput, 9*(4), 837–858.

Yen, S. C., Finkel, L. H. (1998): Extraction of perceptually salient contours by striate cortical networks. *Vision Res, 38*(5), 719–741.

Supporting Information 1

Test images and statistical properties

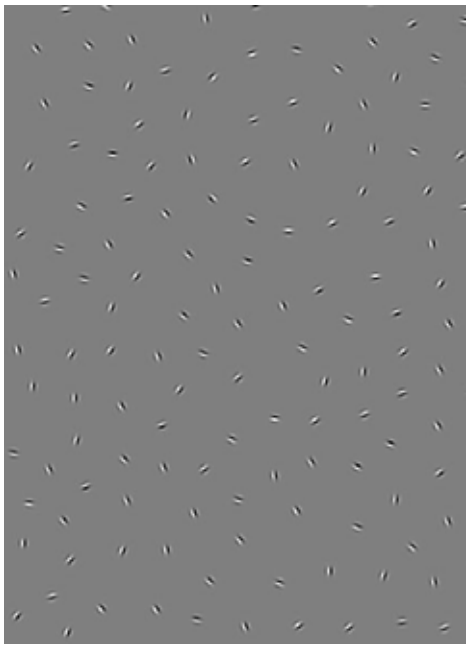

Figure S1C

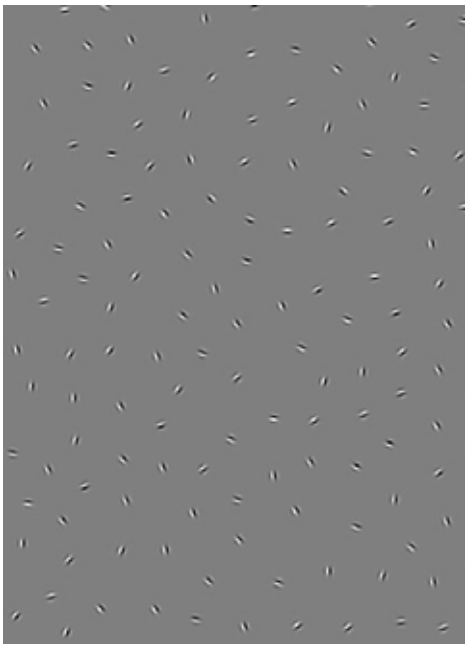

Figure S1O

Picture 1	No.	Distance			
		Min.	Max.	Avg.	Std.
Pattern	13	6.1	7.7	7.0	0.4
Background	119	6.3	10.2	8.4	0.5
All	132	6.1	10.2	8.4	0.5
	No.	Collinearity			
		Min.	Max.	Avg.	Std.
Pattern	13	11.4	34.8	27.0	6.0
Background	119	0.0	90.0	57.6	19.0
All	132	0.0	90.0	57.6	19.0

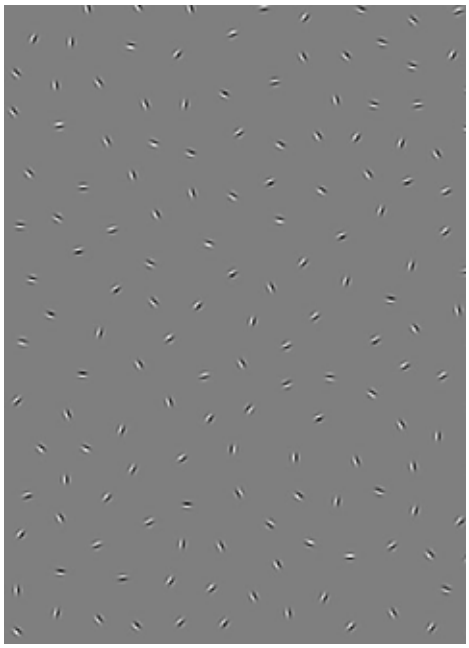

Figure S2C

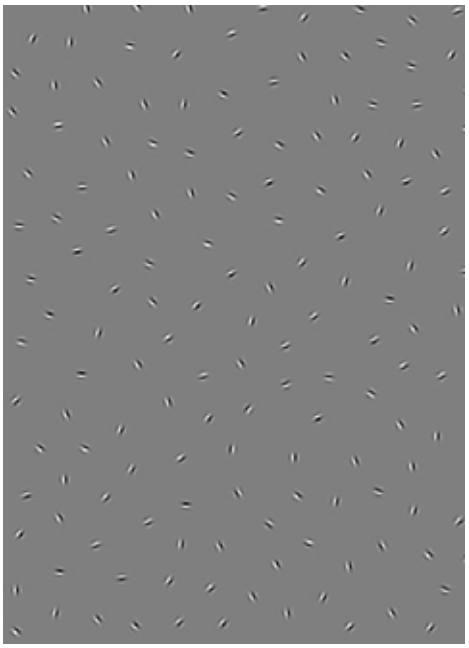

Figure S2O

Picture 2	No.	Distance			
		Min.	Max.	Avg.	Std.
Pattern	13	6.6	7.4	7.0	0.2
Background	132	5.8	10.3	8.1	0.6
All	145	5.8	10.3	8.1	0.6
	No.	Collinearity			
		Min.	Max.	Avg.	Std.
Pattern	13	8.9	36.9	22.8	6.4
Background	132	0.0	90.0	58.6	18.2
All	145	0.0	90.0	58.5	18.2

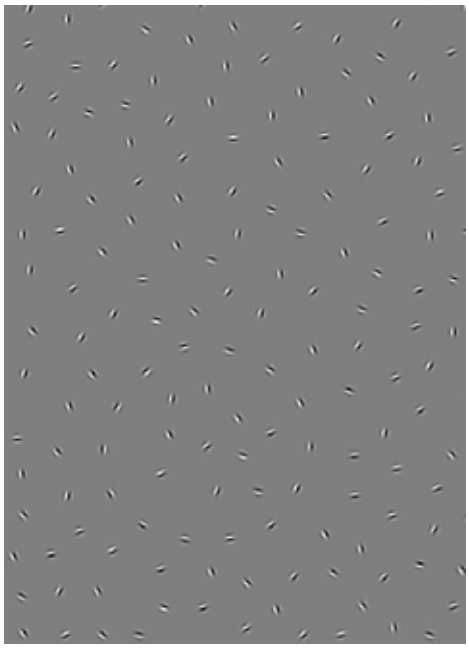

Figure S3C

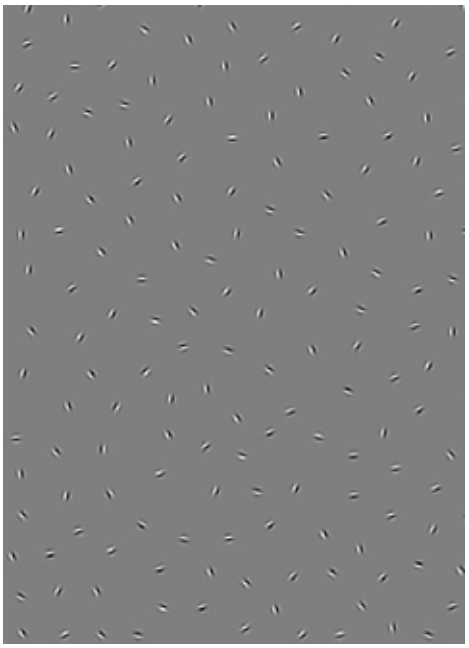

Figure S3O

Picture 3	No.	Distance			
		Min.	Max.	Avg.	Std.
Pattern	14	6.5	7.4	7.0	0.2
Background	140	5.1	9.8	7.7	0.6
All	154	5.1	9.8	7.7	0.6
	No.	Collinearity			
		Min.	Max.	Avg.	Std.
Pattern	14	11.8	29.7	19.1	4.8
Background	140	0.0	90.0	57.7	19.3
All	154	0.0	90.0	57.5	19.3

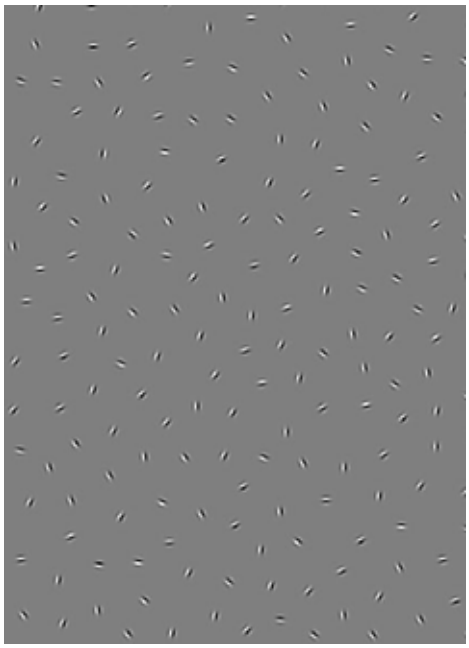

Figure S4C

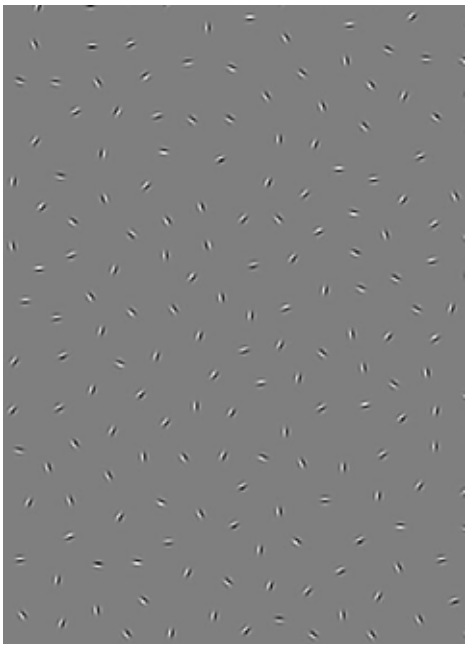

Figure S4O

Picture 4	No.	Distance			
		Min.	Max.	Avg.	Std.
Pattern	13	6.6	7.5	7.0	0.2
Background	155	5.4	9.3	7.4	0.5
All	168	5.4	9.3	7.3	0.5
	No.	Collinearity			
		Min.	Max.	Avg.	Std.
Pattern	13	10.3	38.3	23.4	7.2
Background	155	0.1	90.0	56.8	18.9
All	168	0.1	90.0	56.7	19.0

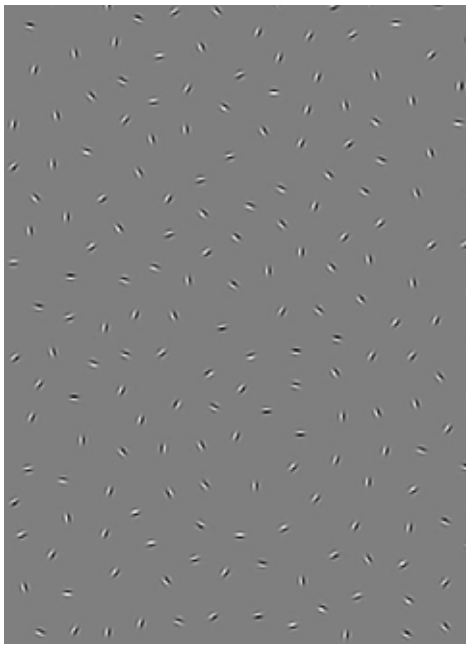

Figure S5C

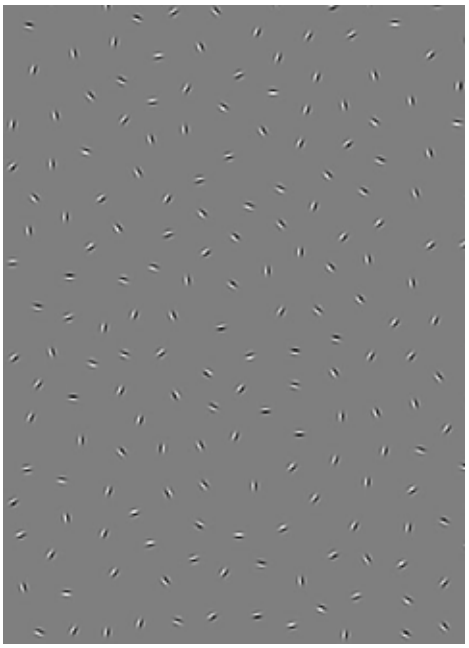

Figure S5O

Picture 5	No.	Distance			
		Min.	Max.	Avg.	Std.
Pattern	13	6.7	7.6	7.1	0.2
Background	163	5.7	8.4	7.0	0.4
All	176	5.7	8.5	7.0	0.3
	No.	Collinearity			
		Min.	Max.	Avg.	Std.
Pattern	13	16.1	32.9	23.1	4.2
Background	163	0.0	90.0	58.4	18.5
All	176	0.0	90.0	58.4	18.5

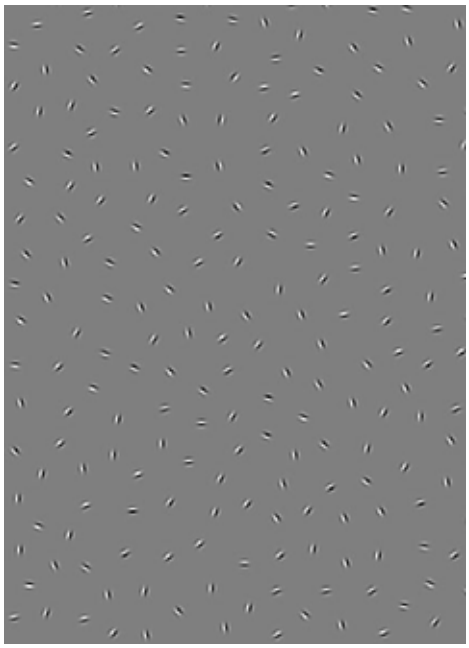

Figure S6C

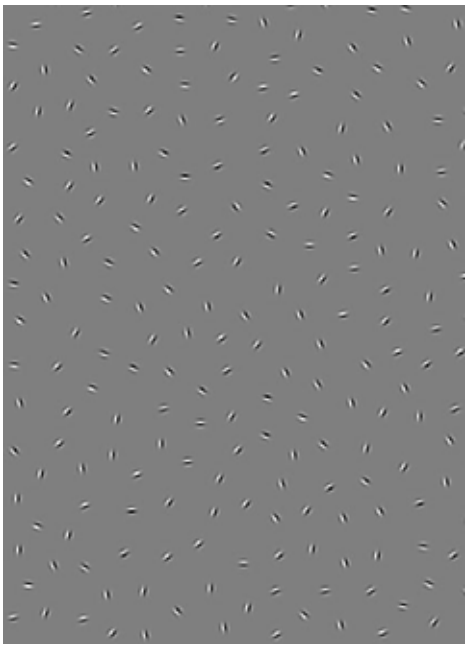

Figure S6O

Picture 6	No.	Distance			
		Min.	Max.	Avg.	Std.
Pattern	13	6.8	7.4	7.0	0.2
Background	183	5.5	7.8	6.7	0.3
All	196	5.5	7.8	6.7	0.3
	No.	Collinearity			
		Min.	Max.	Avg.	Std.
Pattern	13	8.5	35.2	21.9	6.2
Background	183	0.0	90.0	58.2	19.2
All	196	0.0	90.0	58.1	19.2

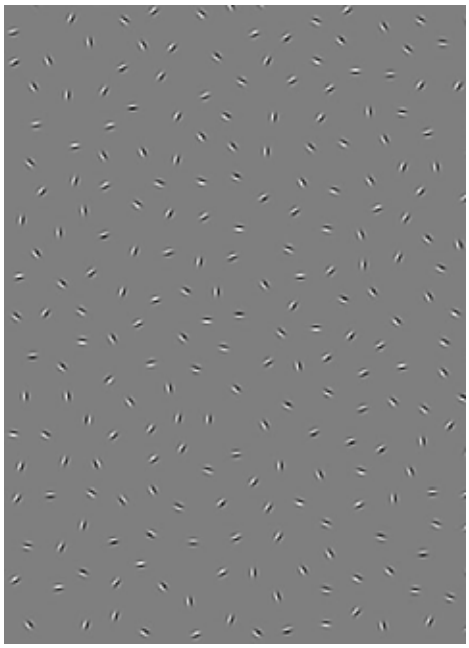

Figure S7C

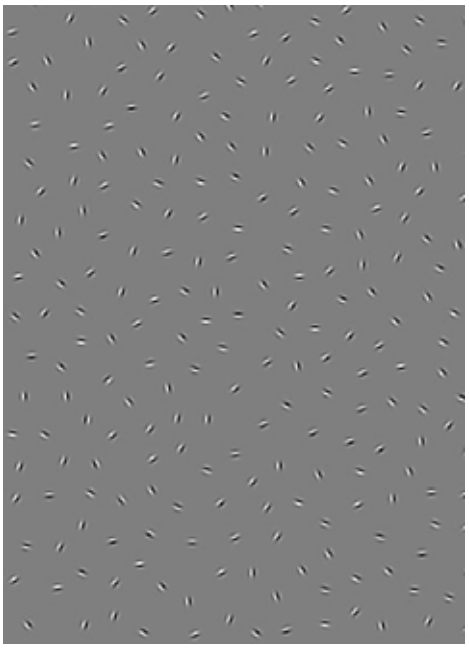

Figure S7O

Picture 7	No.	Distance			
		Min.	Max.	Avg.	Std.
Pattern	13	6.6	7.6	7.0	0.2
Background	211	4.2	8.4	6.3	0.5
All	224	4.2	8.4	6.3	0.5
	No.	Collinearity			
		Min.	Max.	Avg.	Std.
Pattern	13	12.0	32.5	22.2	6.5
Background	211	0.0	90.0	58.6	18.8
All	224	0.0	90.0	58.6	18.8

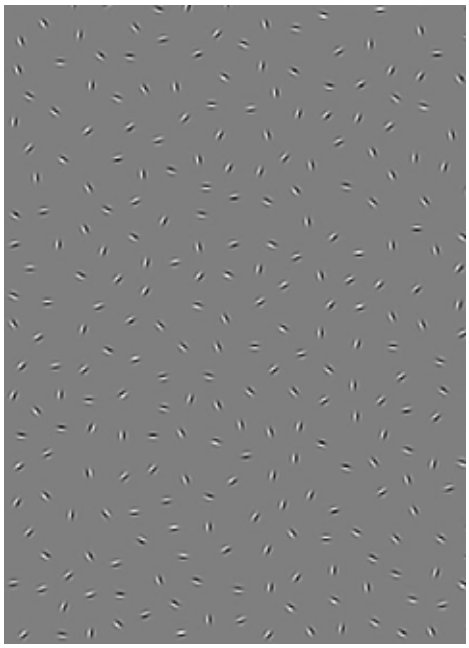

Figure S8C

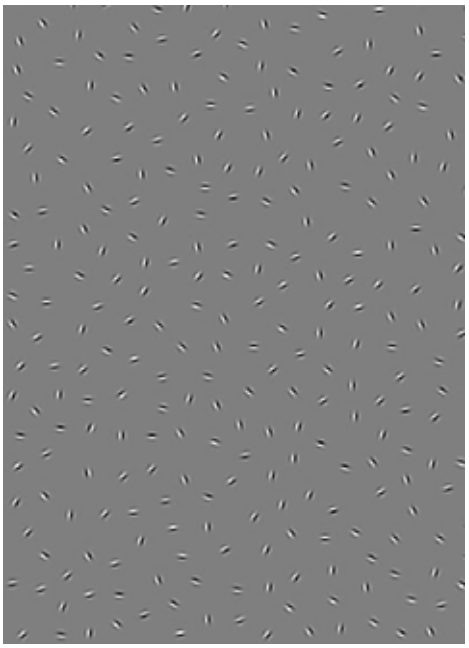

Figure S8O

Picture 8	No.	Distance			
		Min.	Max.	Avg.	Std.
Pattern	13	6.8	7.3	7.0	0.1
Background	247	4.3	7.5	5.9	0.4
All	260	4.3	7.5	5.9	0.4
	No.	Collinearity			
		Min.	Max.	Avg.	Std.
Pattern	13	12.7	36.1	24.3	6.8
Background	247	0.0	90.0	57.8	19.4
All	260	0.0	90.0	57.7	19.5

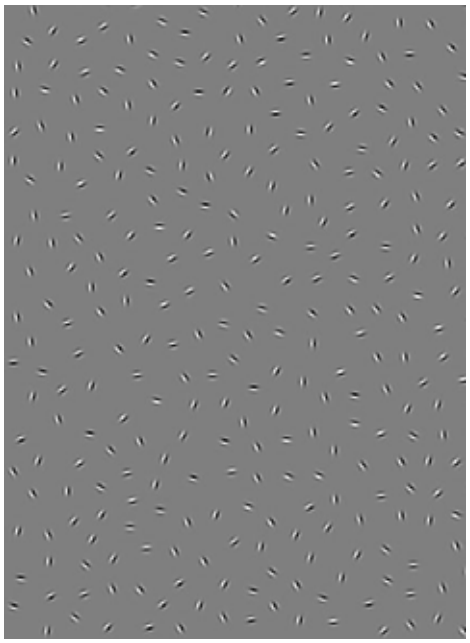

Figure S9C

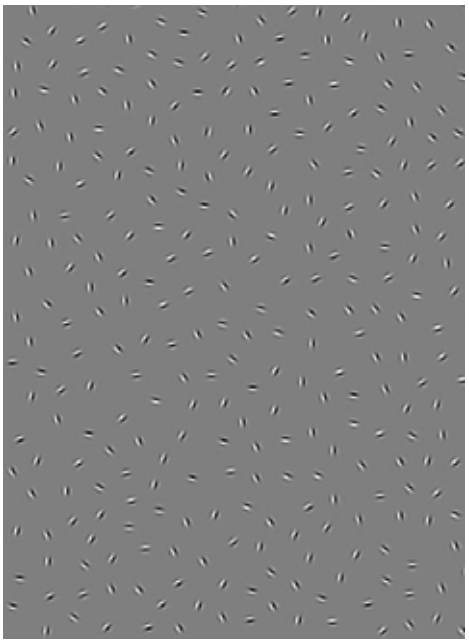

Figure S9O

Picture 9	No.	Distance			
		Min.	Max.	Avg.	Std.
Pattern	14	6.5	7.8	7.1	0.3
Background	275	3.3	7.6	5.6	0.5
All	289	3.3	7.8	5.6	0.5
	No.	Collinearity			
		Min.	Max.	Avg.	Std.
Pattern	14	8.8	30.6	20.7	4.7
Background	275	0.0	90.0	58.2	19.3
All	289	0.0	90.0	58.2	19.3

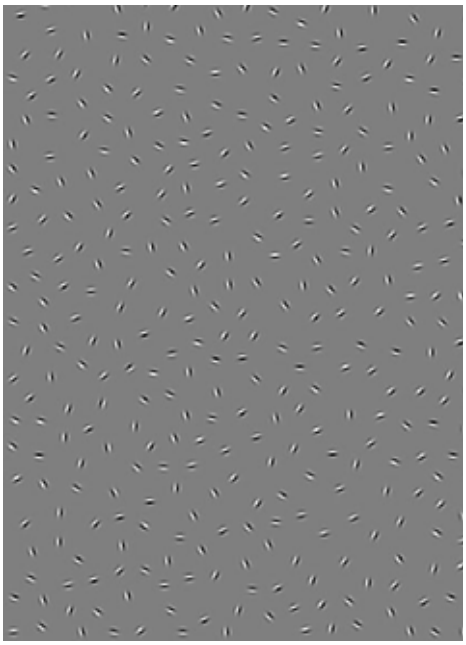

Figure S10C

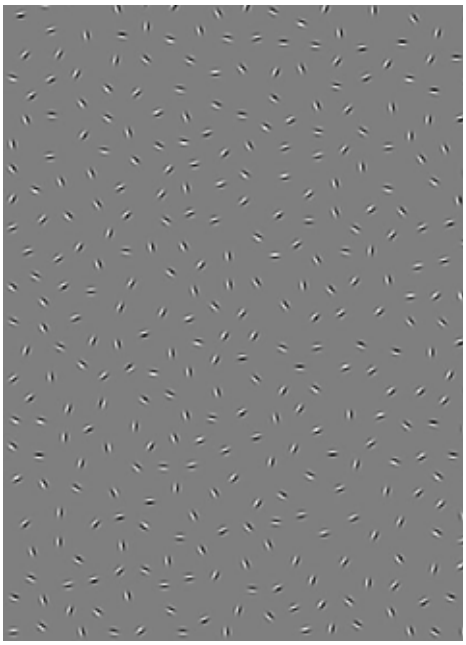

Figure S10O

Picture 10	No.	Distance			
		Min.	Max.	Avg.	Std.
Pattern	13	6.5	7.5	7.0	0.3
Background	318	1.7	9.0	5.2	0.9
All	331	1.7	9.0	5.3	0.9
	No.	Collinearity			
		Min.	Max.	Avg.	Std.
Pattern	13	14.5	34.5	23.5	4.5
Background	318	0.0	90.0	57.7	18.9
All	331	0.0	90.0	57.8	18.9

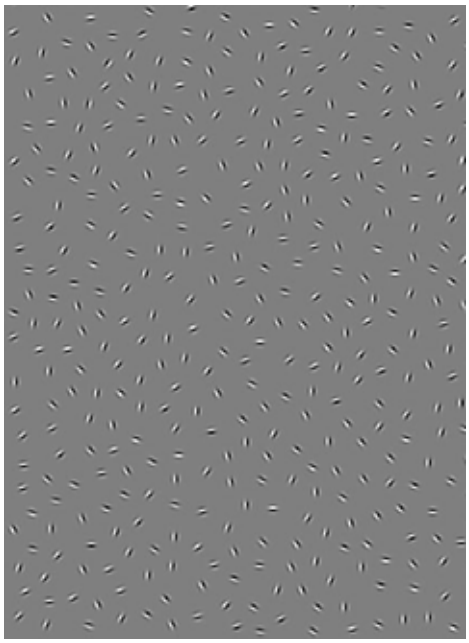

Figure S11C

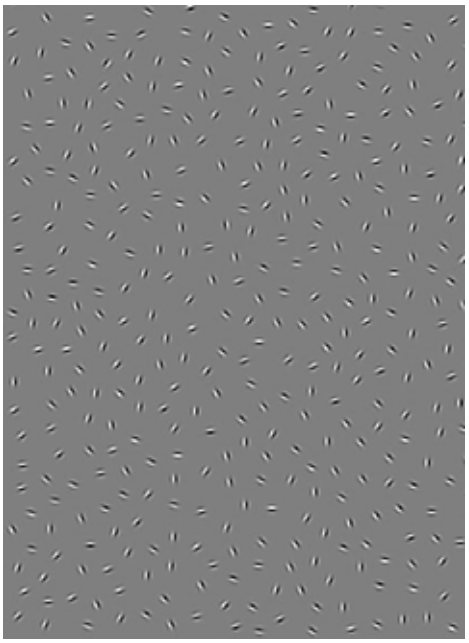

Figure S11O

Picture 11	No.	Distance			
		Min.	Max.	Avg.	Std.
Pattern	14	6.8	7.3	7.1	0.1
Background	364	3.4	6.1	4.9	0.3
All	378	3.4	7.3	4.9	0.3
	No.	Collinearity			
		Min.	Max.	Avg.	Std.
Pattern	14	10.8	30.9	18.9	4.9
Background	364	0.0	90.0	57.7	18.8
All	378	0.0	90.0	57.7	18.8

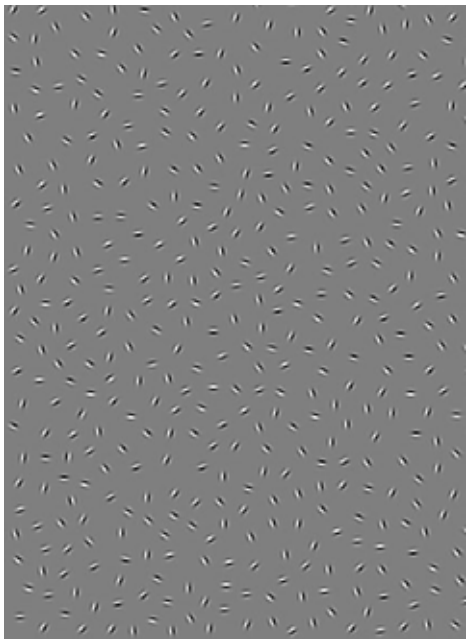

Figure S12C

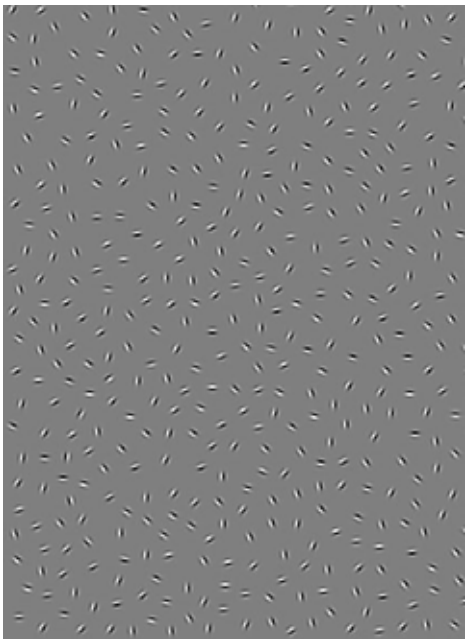

Figure S12O

Picture 12	No.	Distance			
		Min.	Max.	Avg.	Std.
Pattern	14	6.6	7.5	7.0	0.2
Background	415	3.5	5.6	4.5	0.2
All	429	3.5	7.5	4.5	0.3
	No.	Collinearity			
		Min.	Max.	Avg.	Std.
Pattern	14	12.5	29.0	22.3	4.2
Background	415	0.0	90.0	58.0	18.7
All	429	0.0	90.0	58.0	18.7

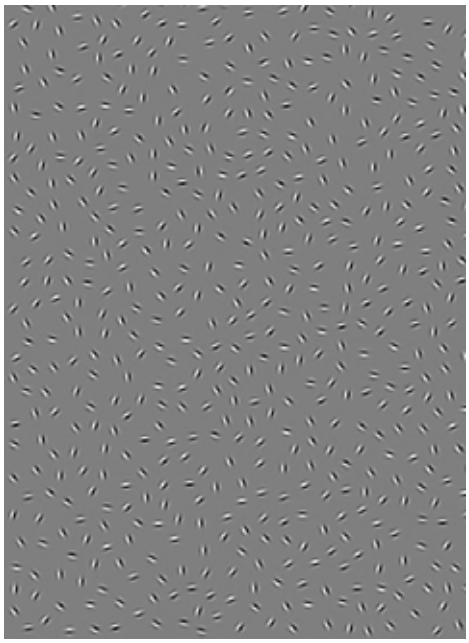

Figure S13C

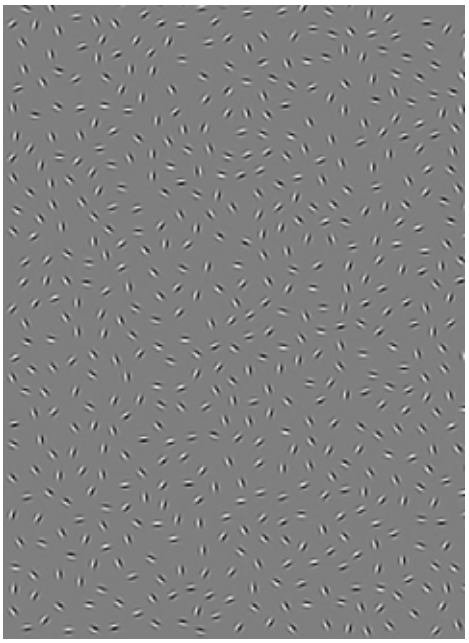

Figure S13O

Picture 13	No.	Distance			
		Min.	Max.	Avg.	Std.
Pattern	13	6.7	7.4	7.0	0.2
Background	541	2.8	5.6	4.2	0.3
All	554	2.8	7.4	4.2	0.3
	No.	Collinearity			
		Min.	Max.	Avg.	Std.
Pattern	13	8.2	29.3	19.2	5.3
Background	541	0.0	90.0	58.1	19.4
All	554	0.0	90.0	58.1	19.3

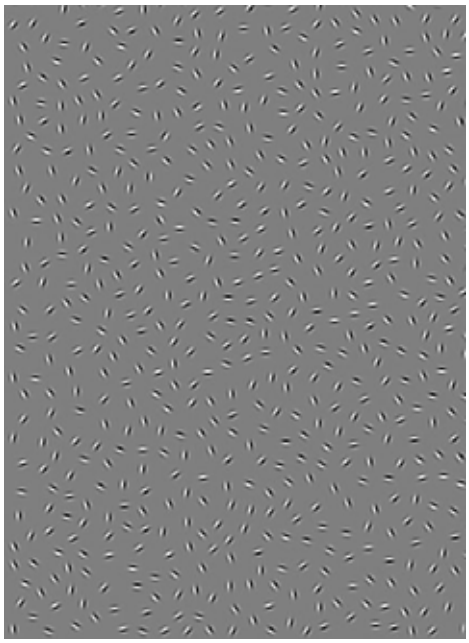

Figure S14C

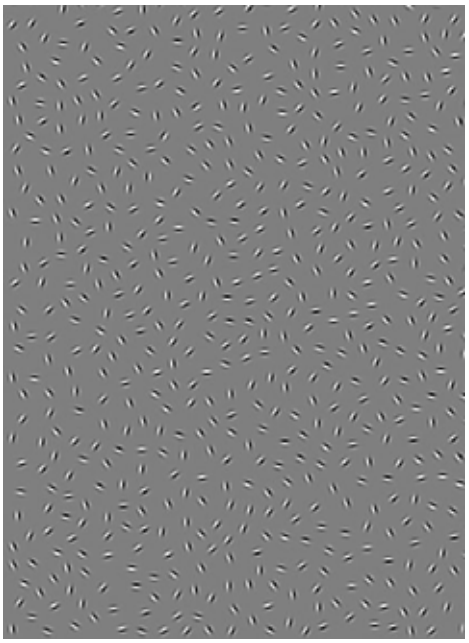

Figure S14O

Picture 14	No.	Distance			
		Min.	Max.	Avg.	Std.
Pattern	13	6.8	7.6	7.2	0.2
Background	576	3.2	4.6	3.8	0.1
All	589	3.2	7.6	3.8	0.2
	No.	Collinearity			
		Min.	Max.	Avg.	Std.
Pattern	13	9.4	30.9	19.6	6.8
Background	576	0.0	90.0	58.3	18.8
All	589	0.0	90.0	58.3	18.8

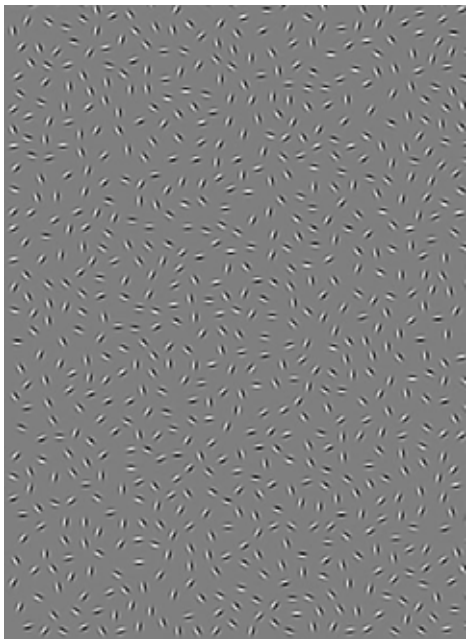

Figure S15C

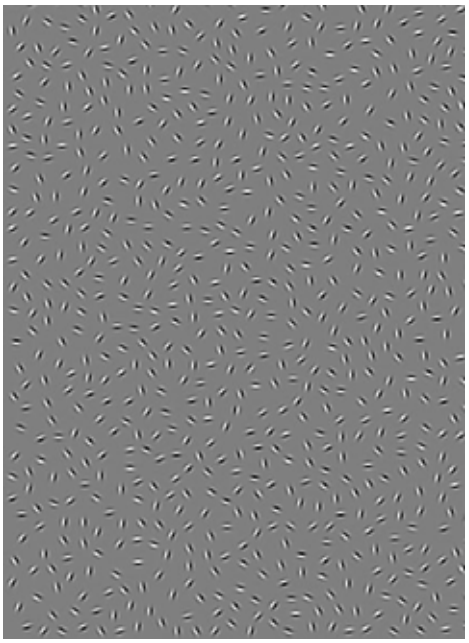

Figure S15O

Picture 15	No.	Distance			
		Min.	Max.	Avg.	Std.
Pattern	13	6.3	7.4	7.0	0.3
Background	710	2.7	4.2	3.5	0.2
All	723	2.7	7.4	3.5	0.2
	No.	Collinearity			
		Min.	Max.	Avg.	Std.
Pattern	13	7.9	37.7	18.9	7.3
Background	710	0.0	90.0	58.2	18.8
All	723	0.0	90.0	58.2	18.8

Supporting Information 2

Additional analysis of the algorithm

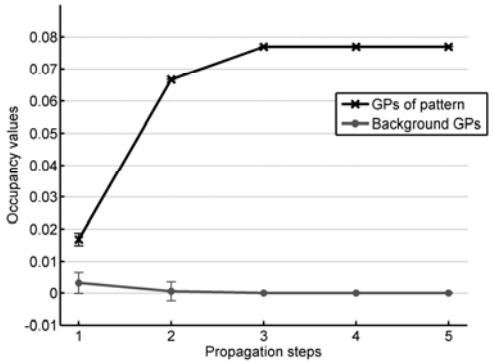

Figure S2_1. The change of the average occupancy values during the propagation steps, calculated on Image 8C (Figure S8, the same figure as seen on Figure 3. from the article). The overall behavior of the model for the same image is shown in Figure 3. The error bars indicate standard deviation.

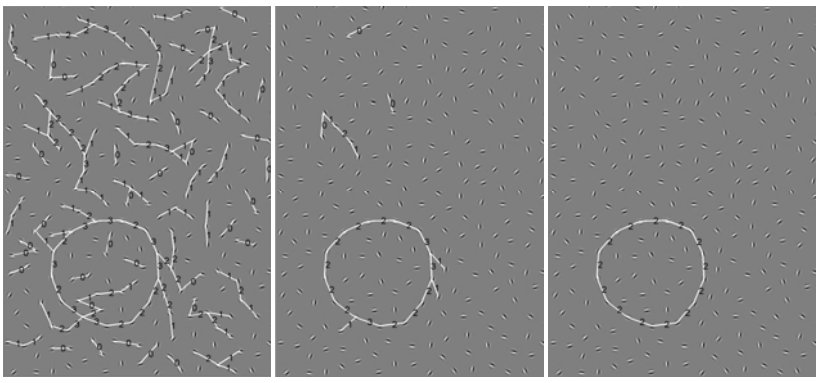

Edges in propagation step 1. Edges in propagation step 2. Edges in propagation step 3.
Figure S2_2 The change of cp - the number of collinear edge pairs that an edge participates in – during the propagation steps. The process is shown on Image 8C (Figure S8). The numbers represent cp values for the edge in question. During the iteration steps, edges with cp=0 are eliminated in Step 2 of the algorithm (construction of the weight matrix) while edges of low occupancy are eliminated in Step 5 (see Algorithm 1).